In situ and *in silico* kinetic analyses of programmed cell death-1 (PD-1) receptor, programmed cell death ligands, and B7-1 protein interaction network

Received for publication, October 18, 2016, and in revised form, March 6, 2017 Published, Papers in Press, March 6, 2017, DOI 10.1074/jbc.M116.763888

Kaitao Li[‡], Xiaoxiao Cheng[§], Andreas Tilevik[¶], Simon J. Davis[§], and Cheng Zhu[‖1]

From the [‡]Coulter Department of Biomedical Engineering, Georgia Institute of Technology, Atlanta 30332-0535, Georgia, the [§]Radcliffe Department of Medicine and Medical Research Council Human Immunology Unit, University of Oxford, John Radcliffe Hospital, Headington, Oxford OX3 9DU, United Kingdom, the [¶]Systems Biology Research Centre, School of Bioscience, University of Skövde, Box 408, Skövde, Sweden, and the [‖]Coulter Department of Biomedical Engineering, the Woodruff School of Mechanical Engineering, and the Institute for Bioengineering and Bioscience, Georgia Institute of Technology, Atlanta 30332-0535, Georgia

Edited by Norma Allewell

Programmed cell death-1 (PD-1) is an inhibitory receptor with an essential role in maintaining peripheral tolerance and is among the most promising immunotherapeutic targets for treating cancer, autoimmunity, and infectious diseases. A complete understanding of the consequences of PD-1 engagement by its ligands, PD-L1 and PD-L2, and of PD-L1 binding to B7-1 requires quantitative analysis of their interactions at the cell surface. We present here the first complete *in situ* kinetic analysis of the PD-1/PD-ligands/B7-1 system. Consistent with previous solution measurements, we observed higher *in situ* affinities for human (h) than murine (m) PD-1 interactions, stronger binding of hPD-1 to hPD-L2 than hPD-L1, and comparable binding of mPD-1 to both ligands. However, in contrast to the relatively weak solution affinities, the *in situ* affinities of PD-1 are as high as those of the T cell receptor for agonist pMHC and of LFA-1 (lymphocyte function-associated antigen 1) for ICAM-1 (intercellular adhesion molecule 1) but significantly lower than that of the B7-1/CTLA-4 interaction, suggesting a distinct basis for PD-1- *versus* CTLA-4-mediated inhibition. Notably, the *in situ* interactions of PD-1 are much stronger than that of B7-1 with PD-L1. Overall, the *in situ* affinity ranking greatly depends on the on-rate instead of the off-rate. *In silico* simulations predict that PD-1/PD-L1 interactions dominate at interfaces between activated T cells and mature dendritic cells and that these interactions will be highly sensitive to the dynamics of PD-L1 and PD-L2 expression. Our results provide a kinetic framework for better understanding inhibitory PD-1 activity in health and disease.

PD-1[2] (CD279) is an immune checkpoint receptor expressed mainly on activated T cells and B cells. Its primary function is to maintain peripheral tolerance within the adaptive immune system. PD-1 deficiency results in spontaneous development of autoimmunity in mouse models (1, 2), and polymorphism of its gene *PDCD1* in humans is associated with various autoimmune diseases including systemic lupus erythematosus, rheumatoid arthritis, type I diabetes, etc., among different populations (3). High surface expression of PD-1 has also been found to be a hallmark of T cell exhaustion, where antigen-specific $CD8^+$ T cells lose their ability to combat tumor cells or virus-infected cells (4, 5). Antibody blockade of the PD-1 pathway is able to restore the effector functions of exhausted $CD8^+$ T cells for tumor or viral clearance, and this approach is emerging as a promising immunotherapeutic strategy to treat a wide range of cancer and infectious diseases, *e.g.* nivolumab and pembrolizumab among others in the pipeline (3, 6). In addition, the more complex functions of PD-1 are evidenced by its important role in the generation and activity of induced regulatory T cells (7–9), its high expression on follicular helper $CD4^+$ T cells (10), the improved cognitive performance in an Alzheimer's mouse model with PD-1 blockade (11), and its expression and growth-promoting effect on certain tumor cells (12).

PD-1 is a type I transmembrane glycoprotein with a single IgV domain in the extracellular region and two tyrosine-based signaling motifs in the cytoplasmic tail: an immunoreceptor tyrosine-based inhibitory motif and an immunoreceptor tyrosine-based switch motif. The potent inhibitory effect of PD-1 relies on the phosphorylation of the immunoreceptor tyrosine-based switch motif and subsequent recruitment of SHP-2, which attenuates TCR or B cell receptor (BCR) proximal signaling (13). The two ligands, PD-L1 (CD274, B7-H1) and PD-L2 (CD273, B7-DC), are both type I transmembrane glycoproteins, each consisting of an IgV and an IgC domain with high similarities to other B7 family proteins (14–17). Although both ligands inhibit T cell function *in vitro* upon binding to PD-1, their *in vivo* effects are largely governed by their distinct expression patterns, with PD-L1 universally expressed, whereas PD-L2 is restricted to activated antigen-presenting cells (13). Interest-

This work was supported by National Institutes of Health Grant R01AI044902 (to C. Z.). The authors declare that they have no conflicts of interest with the contents of this article. The content is solely the responsibility of the authors and does not necessarily represent the official views of the National Institutes of Health.

[1] To whom correspondence should be addressed: Coulter Department of Biomedical Engineering, 313 Ferst Dr., Georgia Institute of Technology, Atlanta, GA 30332-0535; E-mail: cheng.zhu@bme.gatech.edu.

[2] The abbreviations used are: PD-1, programmed cell death-1; TCR, T cell receptor; ICAM-1, intercellular adhesion molecule 1; LFA-1, lymphocyte function-associated antigen 1; DC, dendritic cell; SA, streptavidin; h-, human; m-, mouse; SPR, surface plasmon resonance; m_r, receptor density; m_l, ligand density.

ingly, the structures of PD-1·PD-ligand complexes manifest the interactions of variable domains from antigen receptors (V_H/V_L for B cell receptor and V_α/V_β for TCR) by using equivalent β-sheets to interact with each other while leaving the loops exposed (18–20). Moreover, a structural comparison of the apo and complexed forms of hPD-1 and mPD-1 reveals significant differences, suggesting potentially distinct ligand binding properties (20, 21). In addition, PD-L1 has been shown to bind B7-1 and induce bidirectional inhibitory signaling in the absence of CD28 and CTLA-4, the previously identified receptors for B7-1 (22).

The great therapeutic potential of PD-1 and its critical role in lymphocyte biology call for a better understanding of the interactions within the complex PD-1/PD-ligands/B7-1 system. Extensive efforts have been made to interrogate these interactions using structural, mutagenesis, and surface plasmon resonance (SPR)-based approaches, establishing our current understanding of the binding interfaces involved, with hotspot regions and potentially distinct binding modes identified and solution binding properties measured (18–20, 23–27). However, most of the kinetic studies used different dimeric protein constructs and reported kinetic parameters with large discrepancies. Recently, Cheng *et al.* (20) characterized in detail the monomeric-binding properties of purified PD-1, PD-ligands, and B7-1 proteins alongside a structural investigation of human PD-1. They reported relatively weak affinities of PD-1/PD-ligand interactions and even lower values for the affinity of the B7-1/PD-L1-binding interactions. We and others have shown that kinetic parameters determined *in situ* with molecules expressed on the native cell membrane display distinct characteristics. In contrast to solution measurements, *in situ* parameters reflect the effective binding properties integrating both the physical and chemical determinants of the binding interface and the modulation of molecular organization by the cellular environment (28). In addition, the *in situ* kinetics of TCR-pMHC interactions have been shown to correlate with antigen recognition and discrimination, signaling, effector function, and developmental fate of T cells better than their counterpart solution parameters (29–34). *In situ* kinetic studies of the PD-1/PD-ligands/B7-1 system will provide us not only a direct description of how they interact on the cell membrane, a key step to delineating the interaction network, but also mechanistic insights as to how *in situ* and solution kinetics would correlate or differ for various molecular interactions.

Here we report a systematic *in situ* kinetic analysis of the PD-1/PD-ligands/B7-1 system in both human and murine species. The *in situ* parameters, although generally exhibiting the same trends as the solution measurements using the same protein constructs, categorize PD-1/PD-ligand binding as intermediate-to-strong interactions based on comparisons with the *in situ* affinities of TCR interacting with agonist pMHC or of activated lymphocyte function-associated antigen 1 (LFA-1) binding to intercellular adhesion molecule 1 (ICAM-1). In addition, the human and murine B7-1/PD-L1 interaction was found to be much weaker than the PD-1/PD-L1 interaction. Finally, simulations based on the kinetic analysis allowed us to delineate the contribution of individual receptor-ligand species to the interaction network, offering a better understanding of the immunological role of this system of interactions.

Results

In situ ligand interactions of human PD-1

The solution binding between monomeric hPD-1 and hPD ligands displays weak solution affinities (μM level K_d) despite the potent inhibitory effect they elicit (20, 24). We performed micropipette adhesion frequency assays (see "Experimental procedures") using CHO cells expressing hPD-1 and RBCs coated with hPD-L1 or hPD-L2 to study their *in situ* interactions (Fig. 1). This assay has previously been confirmed to have single-bond sensitivity yet remains highly specific (35). For CHO cells expressing 128 hPD-1 molecules per μm^2, RBCs coated with hPD-L1 (16.4/μm^2) or hPD-L2 (5.3/μm^2) generated P_a of 0.62 or 0.6, respectively, whereas RBCs coated with SA alone (ligand-free) gave a P_a of <0.1 (Fig. 1*C*). The P_a was also reduced to background level when hPD-1 was blocked using a monoclonal antibody (clone EH12.2H7) or using WT CHO cells without PD-1 expression, further confirming that detected bond formation is specific for the receptor-ligand pair being analyzed.

Both P_a *versus* t_c curves for hPD-L1 and hPD-L2 binding to hPD-1 fitted well to Equation 1 with R^2 of 0.9831 and 0.9987, respectively (see "Experimental procedures") at three combinations of hPD-1 and hPD-ligand densities (Fig. 2, *A* and *B*), indicating that the previously reported monomeric-binding model in solution also applies to binding on the cell surface. The effective *in situ* affinity (A_cK_a) and off-rate (k_{off}) were extracted from the curve-fitting and used to derive the effective on-rate using Equation 2 (see "Experimental procedures"). Comparing the *in situ* kinetic parameters (Fig. 2, *E–G*, *open columns*, *left ordinate*) with their counterparts measured using SPR (Fig. 2, *E–G*, *gray columns*, *right ordinate*) (20), the effective *in situ* affinities follow the same rank order as the solution affinities but show a greater difference between the two ligands, with the A_cK_a for hPD-1/hPD-L2 3.75-fold higher than that of the hPD-1/hPD-L1 interaction (Fig. 2*E*). The A_cK_a values, $4.74 \pm 0.30 \times 10^{-4}$ and $2.12 \pm 0.56 \times 10^{-3}$ μm^4 for hPD-L1 and hPD-L2, respectively, are similar or higher than that of TCR interacting with potent cognate pMHC ($2.4 \pm 0.2 \times 10^{-4}$ μm^4 for OT-I TCR-OVA:H2-K^b; Ref. 29) or strong interactions between activated LFA-1 and ICAM-1 ($3.30 \pm 0.62 \times 10^{-3}$ μm^4) (36). The higher *in situ* affinity of PD-L2 than PD-L1 is caused by a slower off-rate (0.30 ± 0.07 *versus* 0.50 ± 0.03 s^{-1}; Fig. 2*F*) and a faster *in situ* on-rate ($5.55 \pm 0.23 \times 10^{-4}$ *versus* $2.24 \pm 0.17 \times 10^{-4}$ $\mu m^4 s^{-1}$; Fig. 2*G*), both of which have the same rank order as in solution kinetic analysis (20). The *in situ* on-rate is comparable with those of PSGL-1 interacting with P-selectin or L-selectin, where the fast on-rates facilitate the capture and rolling of trafficking leukocytes on endothelial cells (37). These *in situ* kinetic parameters indicate stronger interactions between PD-1 and PD-ligands on the cell surface with slower off-rate and faster on-rates than previously appreciated based on solution measurements with cell-free systems. Our results may account, at least in part, for PD-1's potent inhibition of TCR signaling.

In situ ligand interactions of murine PD-1

We also characterized the *in situ* interactions of mPD-1 expressed on the CHO cell surface with mPD-ligands coated on

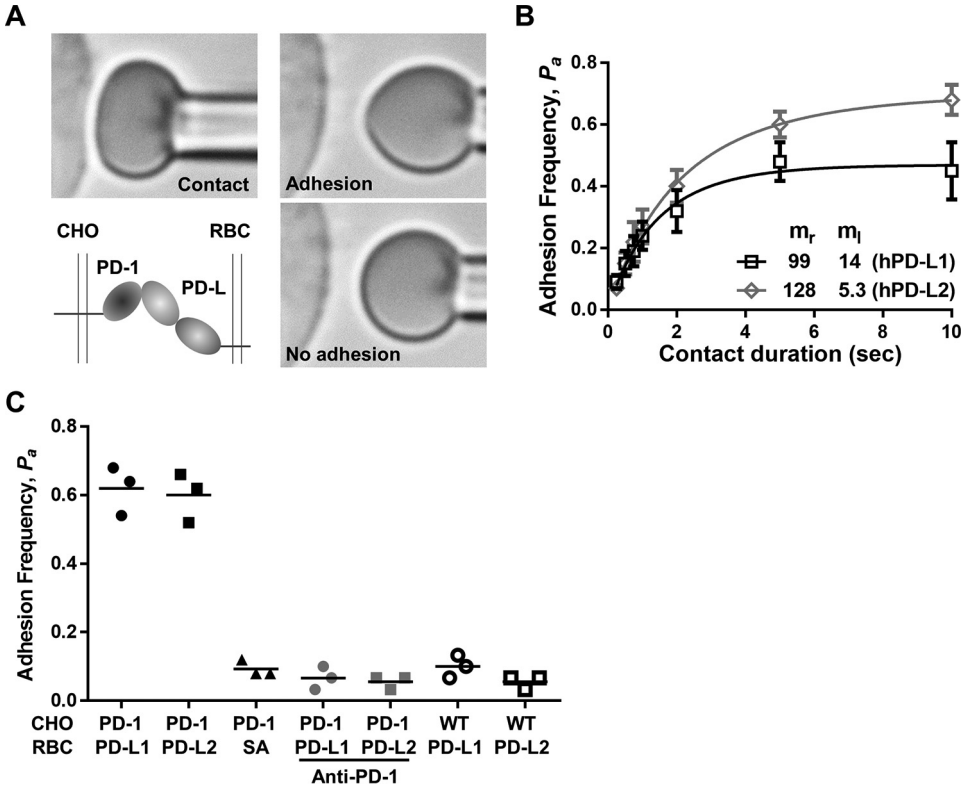

Figure 1. *In situ* kinetic analysis using adhesion frequency assay. *A*, schematics of adhesion frequency assay. A hPD-L1-coated RBC and a CHO cell expressing hPD-1 (*schematic on the lower left*) held by an opposing piezo-driven micropipette were brought into contact for a defined duration (t_c, *upper left*). Upon separation, the test was scored 1 when stretch of the RBC membrane by molecular bond(s) formed during contact was observed (*upper right*) or 0 when no membrane stretch was observed (*lower right*). The same test was repeated 30–50 cycles per cell pair yielding an averaged adhesion frequency, P_a. *B*, adhesion frequency *versus* contact duration curves for hPD-1-ligand interactions. Each point represents the mean ± S.E. of 3–6 cell pairs tested for the corresponding contact duration. *In situ* effective affinity (A_cK_a) and off-rate (k_{off}) were extracted by fitting each curve to Equation 1 in conjugation with measured PD-1 (m_r, #/μm^2) and ligand (m_l, #/μm^2) densities by flow cytometry. *C*, representative specificity controls of adhesion events for hPD-1-ligand interactions including ligand-free RBCs, receptor-free WT CHO cells, or PD-1 CHO cells with anti-PD-1 blocking.

RBCs (Fig. 2, *C* and *D*, Table 1). In contrast to hPD-1, mPD-1 binds to both ligands *in situ* with indistinguishable affinities: $1.69 \pm 0.51 \times 10^{-4}$ and $1.63 \pm 0.34 \times 10^{-4}$ μm^4 for mPD-L1 and mPD-L2, respectively (Fig. 2*E*). However, the same A_cK_a is composed of distinct kinetic rates: mPD-1 binds to mPD-L2 with a 2-fold faster A_cK_{on} and dissociates ~2-fold faster than mPD-L1 (Fig. 2, *F* and *G*). Both *in situ* and solution measurements report lower ligand-binding affinities for mPD-1 than hPD-1 (Fig. 2*E*) (20). The murine to human A_cK_a difference is 2.65-fold for PD-1/PD-L1 but 13-fold for PD-1/PD-L2 interactions (Fig. 2*E*). The reduced *in situ* affinities are largely due to the slower on-rate for mPD-L1 ($5.46 \pm 1.33 \times 10^{-5}$ *versus* $2.24 \pm 0.17 \times 10^{-4}$ μm^{4}s^{-1}) and to both the slower on-rate ($1.59 \pm 0.40 \times 10^{-4}$ *versus* $5.55 \pm 0.23 \times 10^{-4}$ μm^{4}s^{-1}) and faster off-rate (0.97 ± 0.05 s *versus* 0.30 ± 0.07 s) for mPD-L2, compared with the human counterparts.

In situ interactions of PD-L1 with B7-1

PD-L1 has been reported to interact with B7-1 and deliver inhibitory signals bidirectionally (22, 26). However, it remains controversial as to how strong this interaction is compared with PD-1/PD-L1 binding (20, 26). To compare their *in situ* kinetics, we expressed hB7-1 and mB7-1 in CHO cells and tested their binding to PD-L1-coated RBCs. B7-1 has been shown to form non-covalent dimers on the cell surface (38, 39). For both human and murine cases, however, a monomeric binding model (Equation 1) with the same kinetic parameters could be fitted simultaneously to two adhesion frequency curves generated using two sets of molecular densities of B7-1 and PD-L1 (Fig. 3, *A* and *B*), suggesting that dimeric binding did not occur under our experimental conditions (40). The *in situ* affinities are $1.21 \pm 0.16 \times 10^{-5}$ μm^4 for the human interaction and $3.47 \pm 1.25 \times 10^{-6}$ μm^4 for the murine following the same trend as the solution affinities (Fig. 3*C*, Table 1). The higher A_cK_a for hB7-1/hPD-L1 is largely because of its 8.3-fold faster on-rate, although its dissociation is more rapid as well (Fig. 3, *D* and *E*). Interestingly, B7-1/PD-L1 interactions are much weaker than PD-1/PD-L1 interactions, with 37- and 49-fold A_cK_a differences for human and murine, respectively. The differences in the *in situ* parameters are larger than those previously estimated by SPR experiments (20), suggesting that potential restrictions on B7-1/PD-L1 interactions are imposed by the cellular environment. Consistent with this, mPD-L1-coated RBCs generated an adhesion frequency of >50% when tested against activated CD8$^+$ T cells from WT P14 mice, whereas negligible binding was observed in cells from PD-1$^{-/-}$ P14 mice despite the significant levels of B7-1 expressed by both cells (data not shown).

In situ interactions of human B7-1 with CD28 and CTLA-4

To better orient the *in situ* kinetics of the PD-1-ligand interactions, we analyzed the *in situ* interactions of hB7-1 with

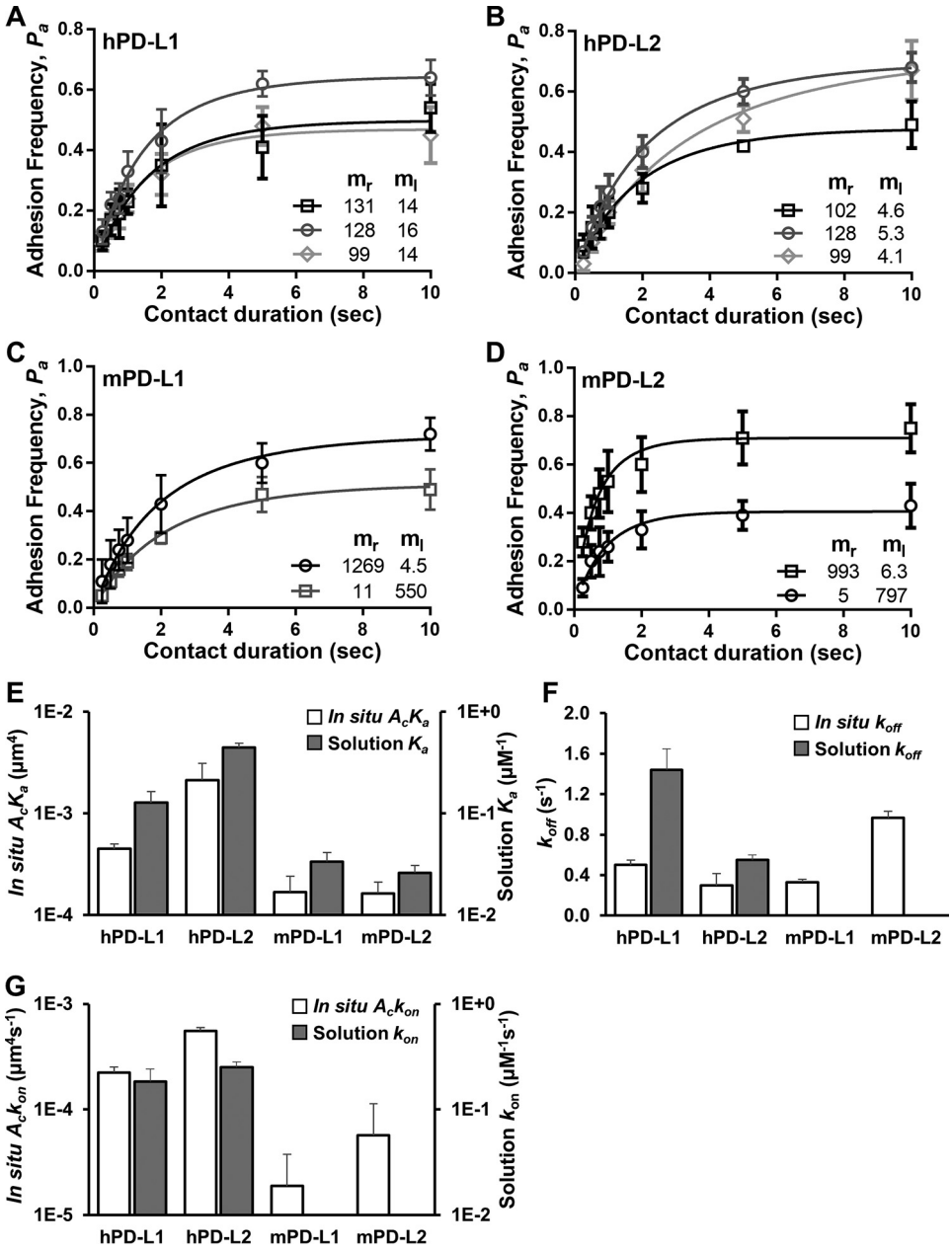

Figure 2. *In situ* and solution kinetics of human and murine PD-1-ligand interactions. *A–D*, adhesion frequency curves of CHO cells expressing hPD-1 (*A* and *B*) or mPD-1 (*C* and *D*) tested against RBCs coated with PD-L1 (*A* and *C*) or PD-L2 (*B* and *D*) of the respective species. Different curves represent independent measurements with different receptor and ligand densities. *E–G*, *in situ* effective affinity (A_cK_a, *E*) *in situ* off-rate (k_{off}, *F*), and *in situ* on-rate (A_cK_{on}, *G*) were derived from data shown in *A–D* using Equations 1 and 2. The corresponding solution kinetics were replotted from published SPR measurements using the same protein constructs (20). Data represent the mean ± S.D. of measurements in *A* and *B*.

Table 1
***In situ* kinetics and affinities of PD-1 and B7-1 interactions**

Interaction	CHO	Purified	A_cK_a	k_{off}	A_ck_{on}
			μm^4	s^{-1}	$\mu m^4 s^{-1}$
hPD-1/PD-L1	hPD-1	hPD-L1	$4.74 \pm 0.30 \times 10^{-4}$	0.50 ± 0.03	$2.24 \pm 0.17 \times 10^{-4}$
hPD-1/PD-L2	hPD-1	hPD-L2	$2.12 \pm 0.56 \times 10^{-3}$	0.30 ± 0.07	$5.55 \pm 0.23 \times 10^{-4}$
hB7–1/PD-L1	hB7-1	hPD-L1	$1.21 \pm 0.16 \times 10^{-5}$	1.31 ± 0.35	$1.52 \pm 0.22 \times 10^{-5}$
hB7–1/CD28	hB7-1	hCD28	$2.68 \pm 0.05 \times 10^{-4}$	1.41 ± 0.20	$3.78 \pm 0.53 \times 10^{-4}$
hB7–1/CTLA-4	hB7-1	hCTLA-4	$1.63 \pm 0.21 \times 10^{-2}$	0.70 ± 0.02	$1.13 \pm 0.001 \times 10^{-2}$
mPD-1/PD-L1	mPD-1	mPD-L1	$1.69 \pm 0.51 \times 10^{-4}$	0.33 ± 0.02	$5.46 \pm 1.33 \times 10^{-5}$
mPD-1/PD-L2	mPD-1	mPD-L2	$1.63 \pm 0.34 \times 10^{-4}$	0.97 ± 0.05	$1.59 \pm 0.40 \times 10^{-4}$
mB7–1/PD-L1	mB7-1	mPD-L1	$3.47 \pm 1.25 \times 10^{-6}$	0.51 ± 0.03	$1.84 \pm 0.74 \times 10^{-6}$

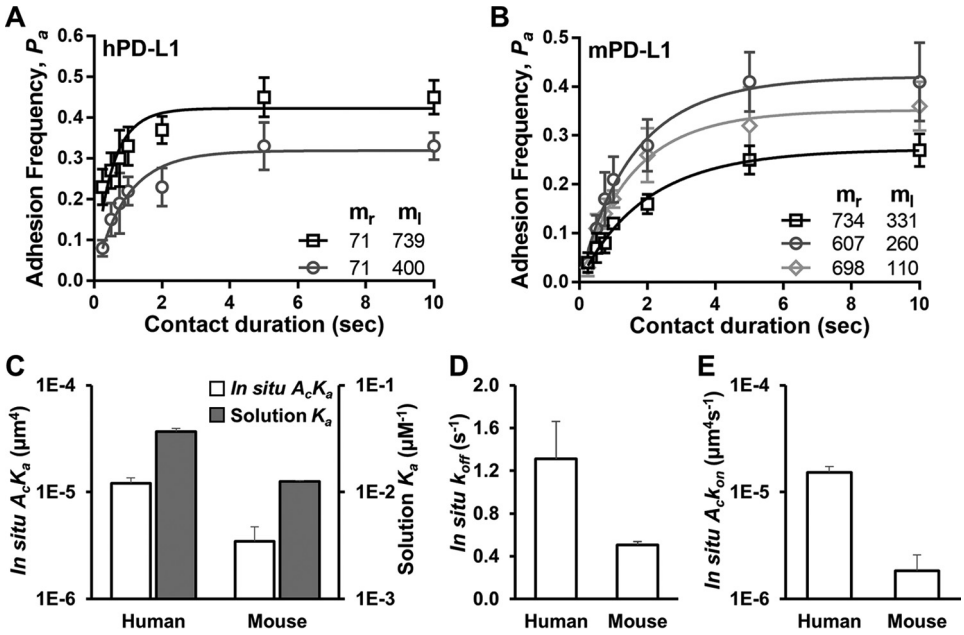

Figure 3. *In situ* and solution kinetics of B7-1/PD-L1 interactions. *A* and *B*, adhesion frequency curves of CHO cells expressing hB7-1 (*A*) or mB7-1 (*B*) tested against RBCs coated with hPD-L1 or mPD-L1, respectively. Different curves represent independent measurements with different receptor and ligand densities. *C–E*, *in situ* effective affinity (A_cK_a, *C*), *in situ* off-rate (k_{off}, *D*), and *in situ* on-rate (A_cK_{on}, *E*) were derived from data shown in *A* and *B* using Equations 1 and 2. The corresponding solution kinetics were replotted from published SPR measurements using the same protein constructs (20). Data represent the mean ± S.D. of measurements in *A* and *B*.

CD28 and CTLA-4, the best-studied interactions in the B7-CD28 family (Fig. 4). CTLA-4 binds to the same ligands as CD28 and antagonizes its costimulatory signaling via multiple mechanisms (41). The kinetic basis manifests as a 10-fold higher solution affinity for B7-1/CTLA-4 (42), which is further enhanced by bivalent binding on the cell membrane (43, 44). The *in situ* affinities follow the same trend but display a 60-fold difference ($2.68 \pm 0.05 \times 10^{-4}$ *versus* $1.63 \pm 0.21 \times 10^{-2}$ μm^4; Fig. 4*C*). Given that low densities of B7-1 were used to reduce dimerization on the membrane, the much larger difference in *in situ* affinity *versus* solution affinity suggests that the *in situ* interactions of these proteins are highly differentially modulated by the cellular environment, *i.e.* native B7-1 is much less favored for binding to CD28 than CTLA-4, potentially due to the membrane constraints (*e.g.* orientation on the membrane) missed in solution measurement. Although the difference in solution affinity was largely attributed to the smaller k_{off} of B7-1/CTLA-4, the *in situ* off-rates are different by only 2-fold (Fig. 4*D*). Instead, the *in situ* on-rate of B7-1/CTLA-4 binding is 50-fold higher than that of that of B7-1/CD28 binding ($1.13 \pm 0.001 \times 10^{-2}$ *versus* $3.78 \pm 0.53 \times 10^{-4}$ $\mu m^4 s^{-1}$; Fig. 4*E*), accounting for the 60-fold higher *in situ* affinity of CTLA-4.

Simulation of complex formation at the T cell/DC interface

Due to the complex nature of the PD-1 and B7-1 network of interactions, the net outcome will depend on the types of complexes formed by each receptor against a background of competition for ligands. To gain quantitative insights into the behavior of this system, we simulated molecular complex formation between an activated human T cell and a mature dendritic cell (DC) by combining receptor and ligand expression levels (20) with the *in situ* binding kinetics measured in this study. Using ordinary differential equations, the model described the process of complex formation involving PD-1 and B7-1 on T cells with PD-L1 and PD-L2 on DC coupled with molecular diffusion of proteins between contacting and non-contacting membrane compartments. The equations and parameter are the same as previously reported (20) except that the kinetic parameters only were used in the present study. Examining the fraction of individual molecular complexes formed reveals the fast establishment (within 30 s) of a steady state over time wherein PD-1/PD-L1 becomes the dominant interaction species (79%) despite its ~3-fold lower *in situ* affinity than PD-1 for PD-L2 (Fig. 5*A*). The dominance of PD-L1 is largely explained by its 15-fold higher (80,372 *versus* 5,243 molecules/cell) expression level *versus* PD-L2 on mature DC (20). Steady-state analysis wherein the number of PD-L1 or PD-L2 on the DC is varied further reveals a range between 2,000 and 200,000 molecules/cell where the fractions of PD-1·PD-L1 and PD-1·PD-L2 complexes changes dramatically (Fig. 5, *B* and *C*). This range is physiologically feasible particularly for PD-L1 (20, 45), suggesting that the contributions of PD-L1 *versus* PD-L2 to complex formation is highly regulated by their expression dynamics. In contrast, increasing B7-1 expression on the T cell did not significantly affect the fraction of PD-1·PD-L1 bonds until reaching a level of >20,000 molecules/cell (Fig. 5*D*), which is much higher than the estimated level of <4,000 molecules/cell (46).

Discussion

The critical role of PD-1 in maintaining peripheral T-cell tolerance and its key suppressive effect on exhausted T cells have made it a promising therapeutic target for restoring T cell functions in a wide range of cancers and infectious diseases. To better understand the biophysicochemical basis of PD-1's function, a spatiotemporal map of ligand binding of PD-1 and

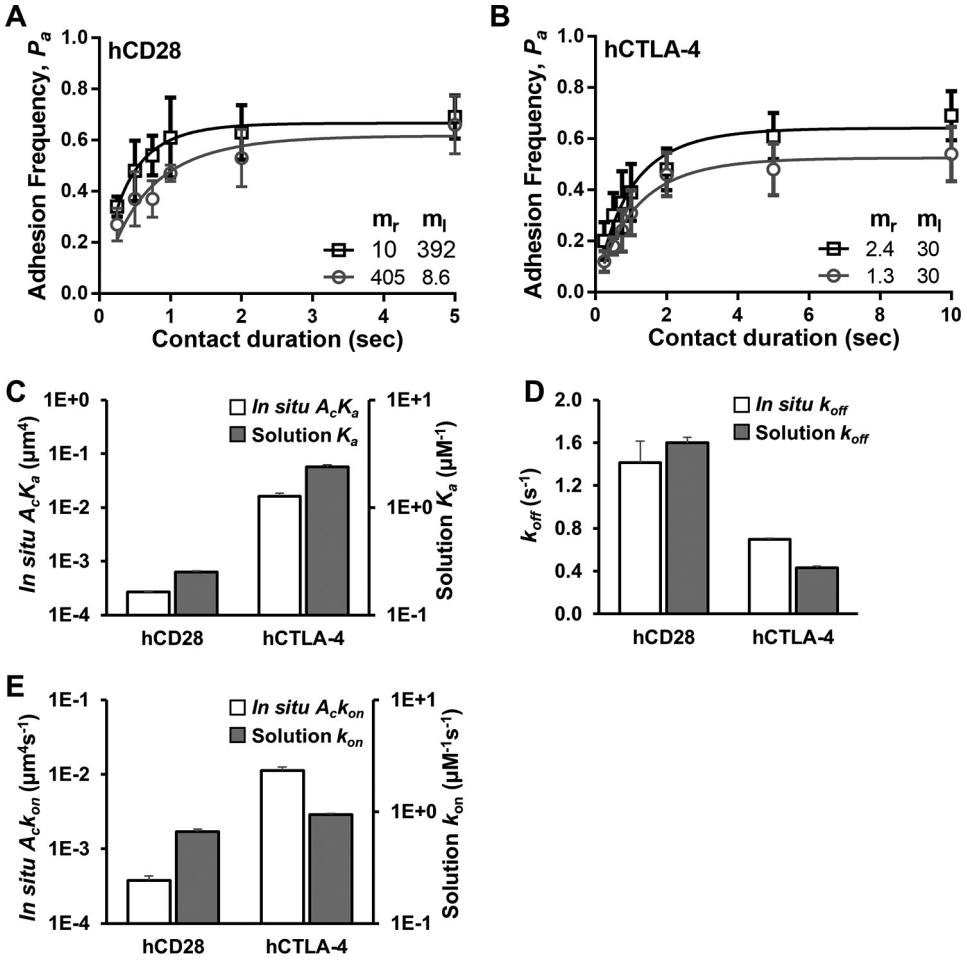

Figure 4. *In situ* and solution kinetics of human B7-1/CD28 and B7-1/CTLA-4 interactions. *A* and *B*, adhesion frequency curves of CHO cells expressing hB7-1 tested against RBCs coated with hCD28 (*A*) or hCTLA-4 (*B*). Different curves represent independent measurements with different receptor and ligand densities. *C–E*, *in situ* effective affinity (A_cK_a, *C*), *in situ* off-rate (k_{off}, *D*), and *in situ* on-rate (A_cK_{on}, *E*) were derived from data shown in *A* and *B* using Equations 1 and 2. The corresponding solution kinetics were replotted from published SPR measurements using the same protein constructs (42). Data represent the mean ± S.D. of measurements in *A* and *B*.

related molecules with specified kinetic properties at the intercellular junction is needed, which have not been reported previously. Here we performed a detailed *in situ* characterization of these kinetics, which combined with the simulation of molecular complex formation at the interface of an activated T cell and a mature DC, provide several insights as discussed below.

Molecular recognition on the T cell membrane is largely governed by the intrinsic properties of the binding sites within a receptor-ligand pair, the net effects on binding of which are usually characterized by SPR analysis or thermodynamic approaches using soluble recombinant polypeptides truncated before the membrane anchor. These measurements in conjunction with structural studies have been invaluable for understanding the binding step of molecular recognition. However, applying the solution-phase results directly to the cellular environment is not necessarily straightforward as at the cell membrane, the orientation, organization, diffusion, and even structures of the proteins are likely to be subject to modulation by the cellular environment. To mimic such physiological situations, we probed the binding to native receptors expressed on the CHO cell membrane with recombinant ligands anchored on the RBC membrane, a configuration better reflecting the representation of the native receptors and a close approximation of the native ligands. We and others have shown in multiple molecular systems that binding kinetics measured *in situ* often differ dramatically from the equivalent solution measurements. For example, the *in situ* kinetics of TCR/pMHC extend over a much wider dynamic range than solution kinetics and correlate better with the functional potency of pMHC ligands (29–34). They are also sensitive to perturbations of the cellular environment such as inhibition of actin polymerization with latrunculin A or disruption of membrane microdomains with cholesterol oxidase (28, 29). Therefore, instead of the intrinsic physicochemical properties of the binding site only, the *in situ* kinetics measured by our assays represent a potentially tunable property of the molecular recognition in the cellular context. The context dependence of such interactions at the very least is illustrated in the molecular interactions measured in this study by the expanded dynamic range of *in situ* affinities compared with their solution counterparts. The solution affinities from the weakest interaction (mB7-1/PD-L1) to the strongest (hB7-1/CTLA-4) spans 200-fold, whereas the *in situ* affinities have a range of almost 4 orders of magnitude (Fig. 6*A*). Interestingly,

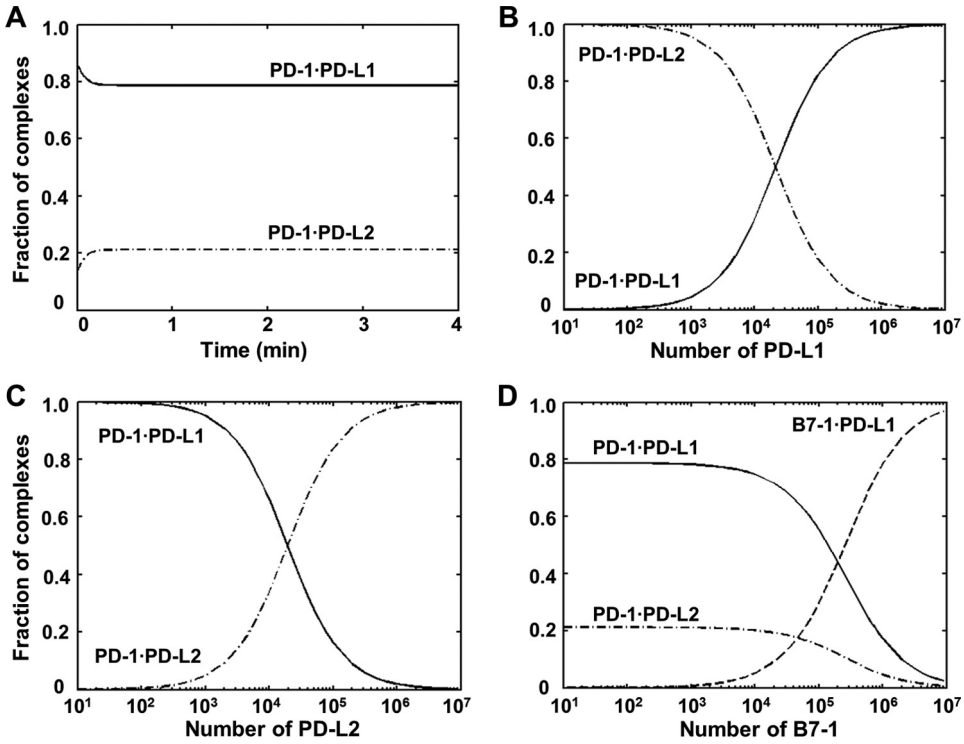

Figure 5. Mathematical simulations of interactions of PD-1, PD-ligands, and B7-1 at the T cell/DC interface. *A*, fraction of PD-1·PD-L1 and PD-1·PD-L2 complexes over time. *B* and *C*, fraction of PD-1·PD-L1 and PD-1·PD-L2 complexes at steady state with varying numbers of PD-L1 (*B*) or PD-L2 (*C*) on the mature DC. *D*, fraction of PD-1·PD-L1, PD-1·PD-L2, and PD-L1·B7-1 complexes at steady state with varying numbers of B7-1 on the activated T cell.

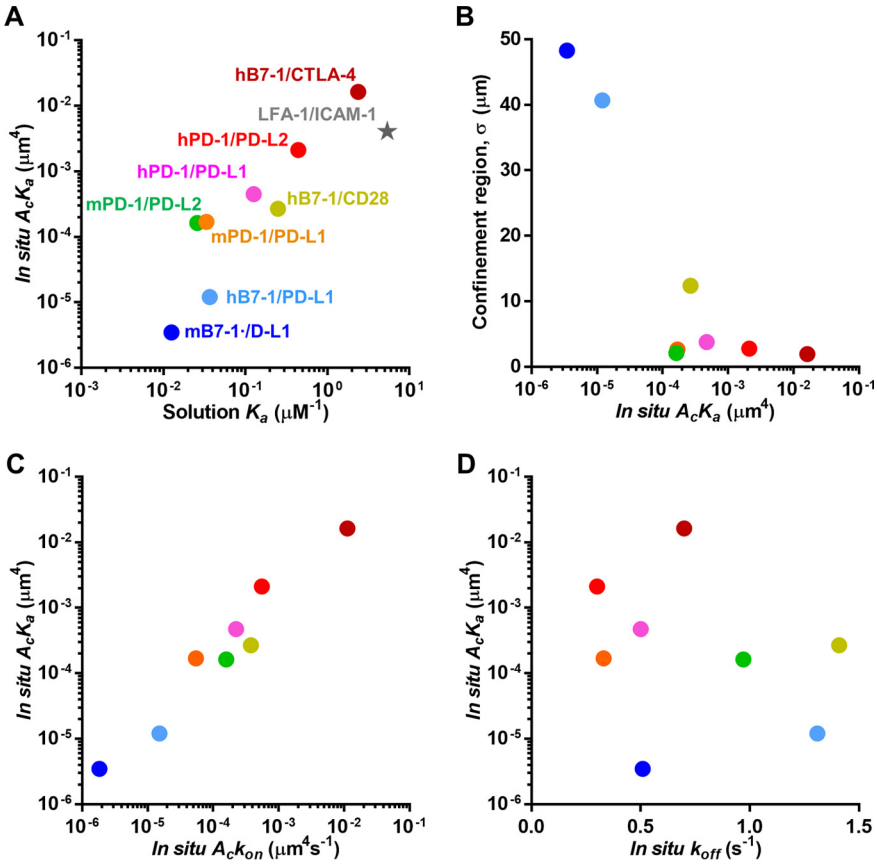

Figure 6. Summary of *in situ* kinetics of PD-1 and B7-1 interactions. *A*, correlation of solution affinity with *in situ* affinity. The solution and *in situ* affinities for LFA-1/ICAM-1 interaction were from Refs. 36 and 51). *B*, calculated confinement lengths according to the Bell model (σ = *in situ* K_d/solution K_d). *C* and *D*, summary of *in situ* on-rate (*C*) and *in situ* off-rate (*D*).

the enhanced dynamic range does not undermine the general agreement between *in situ* and solution measurements, as the ranking of *in situ* affinities correlates almost perfectly with that of the solution measurements (Fig. 6*A*). Neither does the enhancement come from a simple transformation uniformly applied to all interactions. For example, the conversion from solution to *in situ* affinities according to the method of Bell (47, 48) gives variable confinement lengths, a characteristic length reflecting the volume of the search space for molecular binding on the cell surface (Fig. 6*B*). Such variation suggests differential perturbation of *in situ* affinities by the cellular environment. The mechanisms, which are likely complex, may work upon differences in effective molecular length and orientation (48–50). Moreover, it is likely that the *in situ* on-rate, not off-rate, will be subject to the largest effects. The on-rate governs bond formation and hence depends on processes affecting the encounter rate of the interacting molecules at the intercellular junction, which accounts for the major differences in *in situ versus* in-solution binding. The off-rate, on the other hand, is determined by the durability of a bond after it forms and, hence, depends to a greater extent on the physicochemical property at the interface of the molecular complex. This line of reasoning is strongly supported by the remarkable correlation between the *in situ* on-rate and the *in situ* affinity (Fig. 6*C*). The *in situ* on-rate also spans a similar dynamic range as the *in situ* affinity, whereas the *in situ* off-rate changes within a 4-fold range (Fig. 6, *C* and *D*). Overall, our data emphasize the significance and advantages of *in situ* kinetic studies of membrane receptor-ligand interactions, which in contrast to the off-rate dominated solution affinities (20, 42) are more highly dependent on on-rate effects that, as suggested by our data, are a potentially tunable property of the *in situ* interactions.

An important question that has not been fully addressed previously is how strong PD-1-ligand binding as well as PD-L1/B7-1 interactions are compared with the interactions of antigen receptors and other co-stimulatory and co-inhibitory receptors. With enhanced resolution the *in situ* kinetics now defines a more precise ranking of such interactions of interest (Fig. 6*A*). Using the interaction between LFA-1 and ICAM-1 as a reference, the solution K_d is 185 nM when the I-domain of LFA-1 is open, corresponding to the high affinity interaction (51). The solution affinity for the human B7-1/CTLA-4 interaction is moderately lower (K_d = 420 nM). The SPR measurements of bivalent PD-1/PD-ligand interactions (*i.e.* Fc fusion proteins) yielded K_d values ranging from 0.01 μM to 0.8 μM (22, 24, 26, 27), whereas the monomeric interactions are much weaker (K_d = 2–8 μM) (20). In contrast, the *in situ* affinity of B7-1/CTLA-4 is 3-fold higher than that of LFA-1/ICAM-1, and PD-1/PD-ligand *in situ* affinities span the range from intermediate to strong, with the strongest (hPD-1/hPD-L2) comparable to the high affinity LFA-1/ICAM-1 interaction. Similar kinetic advantage for *in situ* binding of these inhibitory receptors is also evident for comparisons based on another co-stimulatory receptor, CD28, interacting with B7-1; *i.e.* interactions that are weaker in solution are similar or even stronger on the cell membrane, whereas the differences of stronger interactions become further amplified, giving rise to 2–5-fold lower confinement lengths than CD28 (Fig. 6*B*). Therefore, the relatively high *in situ* affinities of PD-1/PD-ligand interactions in comparison to the low solution affinities may provide a better understanding of PD-1's potent inhibitory function to counter activating signals by the TCR and co-stimulatory receptors such as CD28. On the other hand, the *in situ* affinities of PD-1-ligand binding are considerably lower than that of CTLA-4, suggesting that distinct mechanisms for their inhibitory effects are at play. This notion is also supported by the fact that CTLA-4 shares the same ligands (B7-1 and B7-2) with the co-stimulatory receptor CD28 and is also evidenced by the different signaling pathways that are thought to act downstream of CTLA-4 and PD-1 (52). Notably, our *in situ* measurements indicate that both human and mouse B7-1/PD-L1 interactions are much weaker than interactions with their canonical receptors; the A_cK_a of B7-1/PD-L1 binding is ~37–49-fold, 20-fold, or 3-log lower than that of PD-1/PD-L1 binding, B7-1/CD28 binding, or B7-1/CTLA-4 binding, respectively. The differences are much larger than the previous solution measurements, manifesting >10-fold higher confinement lengths (Fig. 6*B*). Again, the differences seem to have their source from the *in situ* on-rate instead of off-rate (Fig. 6, *C* and *D*), suggesting that these interactions occur less favorably in the cellular context. Accordingly, *in silico* simulations using these kinetic rates imply that B7-1 will only ever have a negligible effect on the fraction of PD-1·PD-L1 bonds formed at physiological levels of B7-1 expression. These results suggest that these interactions would only be functional when very abundant B7-1 and PD-L1 are present, which then would restrict the significance of this interaction to some particular physiological or pathological conditions in contrast to the broader and more potent effect of PD-1 in maintaining peripheral tolerance. Overall, understanding how these molecules interact *in situ* provides a basis for delineating this network of interactions under physiological conditions, where the interplay is likely to be affected by expression and affinity-based competition and signaling-based cellular regulation. The *in situ* kinetic parameters obtained here would also be a useful source for mathematical simulations of membrane receptor-ligand interactions in pharmacodynamics and thus facilitate drug development targeting this network of molecules.

We found distinct binding kinetics for human *versus* murine PD-1 interactions as well as for PD-L1 *versus* PD-L2 of both species, as also revealed by solution kinetic studies (20, 24, 27). These differential binding properties may be related to the structural differences reported earlier. Compared with mPD-1, hPD-1 has different positioning of the FG loop and also replaces the C″ stand with a flexible loop. Both these regions contribute to ligand binding as shown by an NMR structure (20). The recent structure of a hPD-1·hPD-L1 complex further shows significant plasticity associated with the ligand binding of hPD-1; the CC′ loop that adopts an open conformation in apo-hPD-1 closes upon binding to hPD-L1, whereas the CC′ loop of apo-mPD-1 already displays a closed conformation (21). Also, the two PD-1-ligands may bind to PD-1 via structurally distinct mechanisms. Thermodynamic analysis reveals an entropically driven process for hPD-1/hPD-L1 binding, whereas a large enthalpic term is found for the hPD-1/hPD-L2 interaction (20). All these kinetic and structural differences raise the possibility of differential signaling capacities by PD-L1 *versus* PD-L2. On

the other hand, their functions could be highly regulated by their distinct expression patterns; PD-L1 is universally expressed, whereas PD-L2 expression is restricted to professional antigen-presenting cells. Combining the kinetic and expression profiles, our model simulations demonstrate that the contribution of individual ligands on DCs in forming molecular complexes with PD-1 on T cell is likely to be wholly dominated by their expression dynamics. This result seems to argue against the non-redundant role of PD-1/PD-L2 interaction unless it triggers distinct signaling outcomes by virtue of its enhanced on-rate and capacity for rebinding and its somewhat slower off-rate. Together these structural and kinetic differences between human and murine PD-1 and their interactions with their two ligands imply that PD-1 is subject to continuous selection pressure during evolution, the optimization of which might be critical for balancing immune tolerance with the challenge of dealing with fast-evolving pathogens.

Experimental procedures

Cells and proteins

CHO cells (ATCC) were cultured in RPMI 1640 (Cellgro) supplemented with 10% FBS (Cellgro), 100 units/ml penicillin, 100 μg/ml streptomycin, 2 mM L-glutamine, and 20 mM HEPES and transfected with pcDNA3.1 encoding hPD-1, mPD-1, or hB7-1 using nucleofection (Lonza). To generate stable cell lines, transfected cells were subjected to G418 selection (0.4 mg/ml) and multiple rounds of FACS sorting for uniform surface receptor expression. CHO mB7-1 cells were a generous gift of Dr. Periasamy Selvaraj (Emory University, Atlanta, GA).

His_6-tagged and biotinylatable proteins hPD-L1, hPD-L2, mPD-L1, and mPD-L2 were produced in CHO cells using approaches described previously (42, 53, 54). Biotinylation was performed *in vitro* using the BirA biotin-protein ligase kit (Avidity).

Protein coating on RBC surface

According to a protocol approved by the Institutional Review Board of the Georgia Institute of Technology, human RBCs were isolated from healthy donors, biotinylated with various concentration of Biotin-X-NHS, functionalized with saturating amount of streptavidin (SA), and washed (29). SA-coated RBCs were then incubated with biotinylated recombinant proteins and washed before adhesion frequency assay or flow cytometric analysis.

Site density measurement

CHO cell transfectants and protein-coated RBCs were stained for 30 min at 4 °C in 100 μl of FACS buffer (PBS without Ca^{2+} or Mg^{2+}, 5 mM EDTA, 2% FBS) with 10 μg/ml PE-conjugated antibodies: anti-hPD-1 (clone MIH4), anti-hPD-L1 (clone MIH1), anti-hPD-L2 (clone MIH18), anti-mPD-1 (clone J43), and anti-mB7-1 (clone 1G10/B7) were from BD Pharmingen. Anti-mPD-L1 (clone MIH5), anti-mPD-L2 (clone TY25), and anti-hB7-1 (clone 2D10.4) were from eBioscience. Fluorescently labeled cells together with BD QuantiBRITE PE beads were analyzed using the BD LSR II flow cytometer (BD Biosciences). Molecular site densities were calculated following the instructions of QuantiBRITE PE beads with the cell area derived from diameter measured using cell Multisizer (Beckman Counter).

Adhesion frequency assay

The theoretical framework and detailed procedures have been reported previously (29, 35, 55). As shown in Fig. 1, a CHO-expressing PD-1 and a RBC coated with PD-ligand were repetitively brought in contact for a well defined duration (t_c) with a constant contact area (A_c). Adhesion frequency (P_a) was calculated over scoring 50 contact cycles, with each giving 1 for adhesion or 0 for no adhesion based on the deflection of the RBC membrane upon separation (Fig. 1*A*). The adhesion frequency curve P_a *versus* t_c monotonically increased with contact duration then plateaus, and the P_a *versus* t_c curve changed shape with the PD-1-ligand and level with the receptor (m_r) and ligand (m_l) densities (Fig. 1*B*). This curve reflects the kinetic nature of the molecular bond formation and dissociation at the cellular interface and can be well fitted to the following equation assuming a single step second-order forward, first-order reverse reaction between monomeric receptor and ligand (35).

$$P_a = 1 - \exp\{-m_r m_l A_c K_a[1 - \exp(-k_{off} t_c)] \quad \text{(Eq. 1)}$$

The effective *in situ* affinity ($A_c K_a$) and off-rate (k_{off}) were then determined from least-mean-square fitting in conjunction with measurement of receptor and ligand densities using flow cytometry. *In situ* on-rate was further calculated as

$$A_c k_{on} = A_c K_a \times k_{off} \quad \text{(Eq. 2)}$$

Simulations of complex formation in the PD-1/PD-ligands/B7-1 system

The mathematical model for simulating the interactions of PD-1, PD-1-ligands, and B7-1 has been published previously (20). The same set of equations and parameters was used except for the *in situ* binding kinetics being the numbers measured in this study. Briefly, the model describes the case where an activated T cell expressing PD-1 and B7-1 makes contact with a mature DC with PD-L1 and PD-L2. The molecular interactions at the cell-cell interface and the diffusion across different membrane compartments were integrated into coupled ordinary differential equations. The fraction for each complex in the interface was simulated over time to obtain steady-state values. Analysis of complex fractions at steady-state were examined against varying numbers of PD-L1, PD-L2, or B7-1.

Author contributions—K. L., S. J. D., and C. Z. designed the experiments. K. L. performed most of the experiments. K. L. and C. Z. analyzed the data. X. C. made the recombinant proteins. A. T. performed the *in silico* simulation.

Acknowledgment—We thank Dr. Periasamy Selvaraj (Emory University, Atlanta, GA) for kindly sharing the CHO cell line expressing mouse B7-1.

References

1. Nishimura, H., Nose, M., Hiai, H., Minato, N., and Honjo, T. (1999) Development of lupus-like autoimmune diseases by disruption of the PD-1

gene encoding an ITIM motif-carrying immunoreceptor. *Immunity* **11,** 141–151
2. Nishimura, H., Okazaki, T., Tanaka, Y., Nakatani, K., Hara, M., Matsumori, A., Sasayama, S., Mizoguchi, A., Hiai, H., Minato, N., and Honjo, T. (2001) Autoimmune dilated cardiomyopathy in PD-1 receptor-deficient mice. *Science* **291,** 319–322
3. Okazaki, T., and Honjo, T. (2007) PD-1 and PD-1-ligands: from discovery to clinical application. *Int. Immunol.* **19,** 813–824
4. Barber, D. L., Wherry, E. J., Masopust, D., Zhu, B., Allison, J. P., Sharpe, A. H., Freeman, G. J., and Ahmed, R. (2006) Restoring function in exhausted CD8 T cells during chronic viral infection. *Nature* **439,** 682–687
5. Day, C. L., Kaufmann, D. E., Kiepiela, P., Brown, J. A., Moodley, E. S., Reddy, S., Mackey, E. W., Miller, J. D., Leslie, A. J., DePierres, C., Mncube, Z., Duraiswamy, J., Zhu, B., Eichbaum, Q., Altfeld, M., *et al.* (2006) PD-1 expression on HIV-specific T cells is associated with T-cell exhaustion and disease progression. *Nature* **443,** 350–354
6. Jin, H. T., Ahmed, R., and Okazaki, T. (2011) Role of PD-1 in regulating T-cell immunity. *Curr. Top. Microbiol. Immunol* **350,** 17–37
7. Wang, L., Pino-Lagos, K., de Vries, V. C., Guleria, I., Sayegh, M. H., and Noelle, R. J. (2008) Programmed death 1 ligand signaling regulates the generation of adaptive Foxp3+CD4+ regulatory T cells. *Proc. Natl. Acad. Sci. U.S.A.* **105,** 9331–9336
8. Francisco, L. M., Salinas, V. H., Brown, K. E., Vanguri, V. K., Freeman, G. J., Kuchroo, V. K., and Sharpe, A. H. (2009) PD-L1 regulates the development, maintenance, and function of induced regulatory T cells. *J. Exp. Med.* **206,** 3015–3029
9. Park, H. J., Park, J. S., Jeong, Y. H., Son, J., Ban, Y. H., Lee, B. H., Chen, L., Chang, J., Chung, D. H., Choi, I., and Ha, S. J. (2015) PD-1 up-regulated on regulatory T cells during chronic virus infection enhances the suppression of CD8+ T cell immune response via the interaction with PD-L1 expressed on CD8+ T cells. *J. Immunol.* **194,** 5801–5811
10. Crotty, S. (2011) Follicular helper CD4 T cells (TFH). *Annu. Rev. Immunol.* **29,** 621–663
11. Baruch, K., Deczkowska, A., Rosenzweig, N., Tsitsou-Kampeli, A., Sharif, A. M., Matcovitch-Natan, O., Kertser, A., David, E., Amit, I., and Schwartz, M. (2016) PD-1 immune checkpoint blockade reduces pathology and improves memory in mouse models of Alzheimer's disease. *Nat. Med.* **22,** 135–137
12. Kleffel, S., Posch, C., Barthel, S. R., Mueller, H., Schlapbach, C., Guenova, E., Elco, C. P., Lee, N., Juneja, V. R., Zhan, Q., Lian, C. G., Thomi, R., Hoetzenecker, W., Cozzio, A., Dummer, R., *et al.* (2015) Melanoma cell-intrinsic PD-1 receptor functions promote tumor growth. *Cell* **162,** 1242–1256
13. Keir, M. E., Butte, M. J., Freeman, G. J., and Sharpe, A. H. (2008) PD-1 and its ligands in tolerance and immunity. *Annu. Rev. Immunol.* **26,** 677–704
14. Dong, H., Zhu, G., Tamada, K., and Chen, L. (1999) B7-H1, a third member of the B7 family, co-stimulates T-cell proliferation and interleukin-10 secretion. *Nat. Med.* **5,** 1365–1369
15. Freeman, G. J., Long, A. J., Iwai, Y., Bourque, K., Chernova, T., Nishimura, H., Fitz, L. J., Malenkovich, N., Okazaki, T., Byrne, M. C., Horton, H. F., Fouser, L., Carter, L., Ling, V., Bowman, M. R., *et al.* (2000) Engagement of the PD-1 immunoinhibitory receptor by a novel B7 family member leads to negative regulation of lymphocyte activation. *J. Exp. Med.* **192,** 1027–1034
16. Latchman, Y., Wood, C. R., Chernova, T., Chaudhary, D., Borde, M., Chernova, I., Iwai, Y., Long, A. J., Brown, J. A., Nunes, R., Greenfield, E. A., Bourque, K., Boussiotis, V. A., Carter, L. L., Carreno, B. M., *et al.* (2001) PD-L2 is a second ligand for PD-1 and inhibits T cell activation. *Nat. Immunol.* **2,** 261–268
17. Tseng, S. Y., Otsuji, M., Gorski, K., Huang, X., Slansky, J. E., Pai, S. I., Shalabi, A., Shin, T., Pardoll, D. M., and Tsuchiya, H. (2001) B7-DC, a new dendritic cell molecule with potent costimulatory properties for T cells. *J. Exp. Med.* **193,** 839–846
18. Lázár-Molnár, E., Yan, Q., Cao, E., Ramagopal, U., Nathenson, S. G., and Almo, S. C. (2008) Crystal structure of the complex between programmed death-1 (PD-1) and its ligand PD-L2. *Proc. Natl. Acad. Sci. U.S.A.* **105,** 10483–10488
19. Lin, D. Y., Tanaka, Y., Iwasaki, M., Gittis, A. G., Su, H. P., Mikami, B., Okazaki, T., Honjo, T., Minato, N., and Garboczi, D. N. (2008) The PD-1/PD-L1 complex resembles the antigen-binding Fv domains of antibodies and T cell receptors. *Proc. Natl. Acad. Sci. U.S.A.* **105,** 3011–3016
20. Cheng, X., Veverka, V., Radhakrishnan, A., Waters, L. C., Muskett, F. W., Morgan, S. H., Huo, J., Yu, C., Evans, E. J., Leslie, A. J., Griffiths, M., Stubberfield, C., Griffin, R., Henry, A. J., Jansson, A., *et al.* (2013) Structure and interactions of the human programmed cell death 1 receptor. *J. Biol. Chem.* **288,** 11771–11785
21. Zak, K. M., Kitel, R., Przetocka, S., Golik, P., Guzik, K., Musielak, B., Dömling, A., Dubin, G., and Holak, T. A. (2015) Structure of the complex of human programmed death 1, PD-1, and its ligand PD-L1. *Structure* **23,** 2341–2348
22. Butte, M. J., Keir, M. E., Phamduy, T. B., Sharpe, A. H., and Freeman, G. J. (2007) Programmed death-1 ligand 1 interacts specifically with the B7-1 costimulatory molecule to inhibit T cell responses. *Immunity* **27,** 111–122
23. Wang, S., Bajorath, J., Flies, D. B., Dong, H., Honjo, T., and Chen, L. (2003) Molecular modeling and functional mapping of B7-H1 and B7-DC uncouple costimulatory function from PD-1 interaction. *J. Exp. Med.* **197,** 1083–1091
24. Youngnak, P., Kozono, Y., Kozono, H., Iwai, H., Otsuki, N., Jin, H., Omura, K., Yagita, H., Pardoll, D. M., Chen, L., and Azuma, M. (2003) Differential binding properties of B7-H1 and B7-DC to programmed death-1. *Biochem. Biophys. Res. Commun.* **307,** 672–677
25. Zhang, X., Schwartz, J. C., Guo, X., Bhatia, S., Cao, E., Lorenz, M., Cammer, M., Chen, L., Zhang, Z. Y., Edidin, M. A., Nathenson, S. G., and Almo, S. C. (2004) Structural and functional analysis of the costimulatory receptor programmed death-1. *Immunity* **20,** 337–347
26. Butte, M. J., Peña-Cruz, V., Kim, M. J., Freeman, G. J., and Sharpe, A. H. (2008) Interaction of human PD-L1 and B7-1. *Mol. Immunol.* **45,** 3567–3572
27. Ghiotto, M., Gauthier, L., Serriari, N., Pastor, S., Truneh, A., Nunès, J. A., and Olive, D. (2010) PD-L1 and PD-L2 differ in their molecular mechanisms of interaction with PD-1. *Int. Immunol.* **22,** 651–660
28. Liu, B., Chen, W., Natarajan, K., Li, Z., Margulies, D. H., and Zhu, C. (2015) The cellular environment regulates in situ kinetics of T-cell receptor interaction with peptide major histocompatibility complex. *Eur. J. Immunol.* **45,** 2099–2110
29. Huang, J., Zarnitsyna, V. I., Liu, B., Edwards, L. J., Jiang, N., Evavold, B. D., and Zhu, C. (2010) The kinetics of two-dimensional TCR and pMHC interactions determine T-cell responsiveness. *Nature* **464,** 932–936
30. Liu, B., Zhong, S., Malecek, K., Johnson, L. A., Rosenberg, S. A., Zhu, C., and Krogsgaard, M. (2014) 2D TCR-pMHC-CD8 kinetics determines T-cell responses in a self-antigen-specific TCR system. *Eur. J. Immunol.* **44,** 239–250
31. Hong, J., Persaud, S. P., Horvath, S., Allen, P. M., Evavold, B. D., and Zhu, C. (2015) Force-regulated in situ TCR-peptide-bound MHC class II kinetics determine functions of CD4+ T cells. *J. Immunol.* **195,** 3557–3564
32. Huppa, J. B., Axmann, M., Mörtelmaier, M. A., Lillemeier, B. F., Newell, E. W., Brameshuber, M., Klein, L. O., Schütz, G. J., and Davis, M. M. (2010) TCR-peptide-MHC interactions in situ show accelerated kinetics and increased affinity. *Nature* **463,** 963–967
33. Adams, J. J., Narayanan, S., Liu, B., Birnbaum, M. E., Kruse, A. C., Bowerman, N. A., Chen, W., Levin, A. M., Connolly, J. M., Zhu, C., Kranz, D. M., and Garcia, K. C. (2011) T cell receptor signaling is limited by docking geometry to peptide-major histocompatibility complex. *Immunity* **35,** 681–693
34. Seo, Y. J., Jothikumar, P., Suthar, M. S., Zhu, C., and Grakoui, A. (2016) Local cellular and cytokine cues in the spleen regulate *in situ* T cell receptor affinity, function, and fate of CD8+ T cells. *Immunity* **45,** 988–998
35. Chesla, S. E., Selvaraj, P., and Zhu, C. (1998) Measuring two-dimensional receptor-ligand binding kinetics by micropipette. *Biophys. J.* **75,** 1553–1572
36. Zhang, F., Marcus, W. D., Goyal, N. H., Selvaraj, P., Springer, T. A., and Zhu, C. (2005) Two-dimensional kinetics regulation of $\alpha L\beta 2$-ICAM-1 interaction by conformational changes of the αL-inserted domain. *J. Biol. Chem.* **280,** 42207–42218

37. Chen, W., Evans, E. A., McEver, R. P., and Zhu, C. (2008) Monitoring receptor-ligand interactions between surfaces by thermal fluctuations. *Biophys. J.* **94,** 694–701
38. Bhatia, S., Edidin, M., Almo, S. C., and Nathenson, S. G. (2005) Different cell surface oligomeric states of B7-1 and B7-2: implications for signaling. *Proc. Natl. Acad. Sci. U.S.A.* **102,** 15569–15574
39. James, J. R., Oliveira, M. I., Carmo, A. M., Iaboni, A., and Davis, S. J. (2006) A rigorous experimental framework for detecting protein oligomerization using bioluminescence resonance energy transfer. *Nat. Methods* **3,** 1001–1006
40. Zhang, Y., Jiang, N., Zarnitsyna, V. I., Klopocki, A. G., McEver, R. P., and Zhu, C. (2013) P-selectin glycoprotein ligand-1 forms dimeric interactions with E-selectin but monomeric interactions with L-selectin on cell surfaces. *PloS ONE* **8,** e57202
41. Schildberg, F. A., Klein, S. R., Freeman, G. J., and Sharpe, A. H. (2016) Coinhibitory pathways in the B7-CD28 ligand-receptor family. *Immunity* **44,** 955–972
42. van der Merwe, P. A., Bodian, D. L., Daenke, S., Linsley, P., and Davis, S. J. (1997) CD80 (B7-1) binds both CD28 and CTLA-4 with a low affinity and very fast kinetics. *J. Exp. Med.* **185,** 393–403
43. Stamper, C. C., Zhang, Y., Tobin, J. F., Erbe, D. V., Ikemizu, S., Davis, S. J., Stahl, M. L., Seehra, J., Somers, W. S., and Mosyak, L. (2001) Crystal structure of the B7-1/CTLA-4 complex that inhibits human immune responses. *Nature* **410,** 608–611
44. Ikemizu, S., Gilbert, R. J., Fennelly, J. A., Collins, A. V., Harlos, K., Jones, E. Y., Stuart, D. I., and Davis, S. J. (2000) Structure and dimerization of a soluble form of B7-1. *Immunity* **12,** 51–60
45. Yamazaki, T., Akiba, H., Iwai, H., Matsuda, H., Aoki, M., Tanno, Y., Shin, T., Tsuchiya, H., Pardoll, D. M., Okumura, K., Azuma, M., and Yagita, H. (2002) Expression of programmed death 1 ligands by murine T cells and APC. *J. Immunol.* **169,** 5538–5545
46. Jansson, A., Barnes, E., Klenerman, P., Harlén, M., Sørensen, P., Davis, S. J., and Nilsson, P. (2005) A theoretical framework for quantitative analysis of the molecular basis of costimulation. *J. Immunol.* **175,** 1575–1585
47. Bell, G. I. (1978) Models for the specific adhesion of cells to cells. *Science* **200,** 618–627
48. Dustin, M. L., Bromley, S. K., Davis, M. M., and Zhu, C. (2001) Identification of self through two-dimensional chemistry and synapses. *Annu. Rev. Cell Dev. Biol.* **17,** 133–157
49. Chan, P. Y., and Springer, T. A. (1992) Effect of lengthening lymphocyte function-associated antigen 3 on adhesion to CD2. *Mol. Biol. Cell* **3,** 157–166
50. Huang, J., Chen, J., Chesla, S. E., Yago, T., Mehta, P., McEver, R. P., Zhu, C., and Long, M. (2004) Quantifying the effects of molecular orientation and length on two-dimensional receptor-ligand binding kinetics. *J. Biol. Chem.* **279,** 44915–44923
51. Shimaoka, M., Lu, C., Palframan, R. T., von Andrian, U. H., McCormack, A., Takagi, J., and Springer, T. A. (2001) Reversibly locking a protein fold in an active conformation with a disulfide bond: integrin αL I domains with high affinity and antagonist activity *in vivo*. *Proc. Natl. Acad. Sci. U.S.A.* **98,** 6009–6014
52. Parry, R. V., Chemnitz, J. M., Frauwirth, K. A., Lanfranco, A. R., Braunstein, I., Kobayashi, S. V., Linsley, P. S., Thompson, C. B., and Riley, J. L. (2005) CTLA-4 and PD-1 receptors inhibit T-cell activation by distinct mechanisms. *Mol. Cell. Biol.* **25,** 9543–9553
53. Davis, S. J., Ward, H. A., Puklavec, M. J., Willis, A. C., Williams, A. F., and Barclay, A. N. (1990) High level expression in Chinese hamster ovary cells of soluble forms of CD4 T lymphocyte glycoprotein including glycosylation variants. *J. Biol. Chem.* **265,** 10410–10418
54. Collins, A. V., Brodie, D. W., Gilbert, R. J., Iaboni, A., Manso-Sancho, R., Walse, B., Stuart, D. I., van der Merwe, P. A., and Davis, S. J. (2002) The interaction properties of costimulatory molecules revisited. *Immunity* **17,** 201–210
55. Chen, W., Zarnitsyna, V. I., Sarangapani, K. K., Huang, J., and Zhu, C. (2008) Measuring receptor-ligand binding kinetics on cell surfaces: from adhesion frequency to thermal fluctuation methods. *Cell. Mol. Bioeng.* **1,** 276–288